

# Cavity optomechanical transduction sensing of single molecules

Wenyan Yu,<sup>1,\*</sup> Wei C. Jiang,<sup>2,\*</sup> Qiang Lin,<sup>2,3,†</sup> and Tao Lu<sup>1,‡</sup>

<sup>1</sup>Department of Electrical and Computer Engineering,  
University of Victoria, Victoria, BC V8P 5C2, Canada

<sup>2</sup>Institute of Optics, University of Rochester, Rochester, NY 14627, USA

<sup>3</sup>Department of Electrical and Computer Engineering, University of Rochester, Rochester, NY 14627, USA

We report narrow linewidth optomechanical oscillation of a silica microsphere immersed in a buffer solution. Through a novel optomechanical transduction sensing approach, single 10-nm-radius silica beads and Bovine serum albumin (BSA) protein molecules with a molecular weight of 66 kDalton were detected. This approach predicts the detection of 3.9 kDalton single molecules at a signal-to-noise ratio above unity.

## I. INTRODUCTION

Sensitive detection of a single nanoparticle/molecule is essential for many applications ranging from medical diagnostics, drug discovery, security screening, to environmental science. In the past decades, a variety of approaches have been developed, among which optical detection based on high-Q microcavities has shown significant advantages for its high sensitivity and label-free operation<sup>1-9</sup>. Here, by taking advantage of the intriguing optically induced spring in a silica microsphere, we demonstrate that a quivering cavity can enhance the sensing resolution by orders of magnitude compared with conventional approaches, which allows us to detect single Bovine Serum Albumin (BSA) proteins with a molecular weight of 66 kDalton at a signal-to-noise ratio (SNR) of 16.8. This unique approach opens up a distinctive avenue that not only enables biomolecule sensing and recognition at individual level, but also exhibits great potential for studying/manipulating mechanical properties of individual biomolecules and their interactions.

Binding of a particle to a high-Q optical microcavity perturbs the cavity mode at a resonance wavelength of  $\lambda_0$ , resulting in a cavity resonance shift of  $\delta\lambda$  which in turn changes the cavity transmission. This mechanism underlies the majority of current microcavity sensors, with a sensing resolution dependent critically on the optical quality factor (Q)<sup>10</sup>. To date, the highest resolution reported is a resonance shift of  $(\delta\lambda/\lambda_0) = 3 \times 10^{-10}$  achieved with an optical Q of one hundred million at a visible wavelength in an aqueous environment<sup>5</sup>, which, however, is still larger than that induced by a single protein binding event<sup>3</sup>. Consequently, detection of single protein molecule requires incorporating a plasmonic nanoantenna on the microcavity to enhance the resonance wavelength shift<sup>11-14</sup>, at a price of significant reduction of effective detection area.

On the other hand, the optical wave cycling inside the microcavity is able to produce a radiation pressure that interacts with the mechanical motion of the device (Fig. 1a). Such optomechanical coupling flourishes in profound physics that has

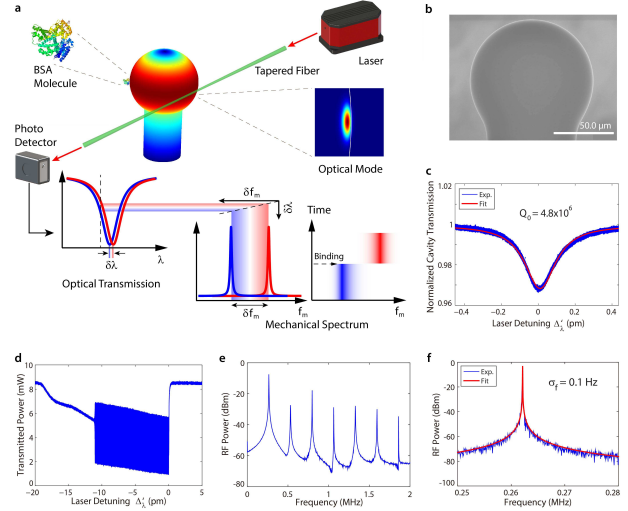


FIG. 1: (a) Schematic illustrating the sensing mechanism. A protein molecule bound to an optomechanically oscillating microsphere yields an optical resonance shift  $\delta\lambda$ , which is transduced to a mechanical frequency shift  $\delta f_m$ . The color map on the microsphere shows the radial breathing mechanical mode simulated by the finite element method. (b) A scanning electron microscopic (SEM) image of a fabricated silica microsphere. (c) The optical transmission spectrum of the microsphere immersed in DPBS, at a probe laser wavelength of 974 nm, with experimental data in blue and theoretical fitting in red. The input power is maintained low enough to characterize the intrinsic optical property of device, which exhibits an intrinsic optical Q of  $4.8 \times 10^6$ . (d) The optical transmission spectrum at an input laser power of 8.5 mW. The coherent OMO was excited with a threshold power of 3.0 mW dropped into the cavity. (e) An example of the power spectral density of the cavity transmission. The fundamental oscillation frequency is located at 262 kHz, with 6 high-order harmonics clearly visible on the spectrum. (f) The detailed spectrum of the fundamental oscillation tone, with experimental data in blue and theoretical fitting in red. The OMO exhibits a full-width at half maximum of 0.1 Hz, corresponding to an effective mechanical Q of  $2.6 \times 10^6$ .

been intensively explored in recent years, particularly in the context of quantum control of mesoscopic mechanical motion<sup>15-19</sup>. When the laser wavelength is blue detuned to the cavity resonance, the optical wave can efficiently boost the mechanical motion above the threshold of regenerative oscillation<sup>15,19</sup>, resulting in highly coherent optomechanical oscil-

\*These authors contributed equally to this work.

†Electronic address: qiang.lin@rochester.edu

‡Electronic address: taolu@ece.uvic.ca

lation (OMO) with a narrow mechanical linewidth. Of particular interest is that the optical wave is able to produce an effective mechanical rigidity whose magnitude depends sensitively on the laser-cavity detuning<sup>19</sup>. Consequently, any tiny perturbation to the cavity resonance wavelength induced by particle/molecule binding would be readily transferred to the frequency shift of the mechanical motion, enabling an efficient transduction mechanism to amplify the resonance wavelength sensing. With the narrow linewidth of coherent OMO, the intriguing optical spring effect would thus offer an elegant approach for sensitive probing of cavity resonance variation, with a sensing resolution given by

$$\left(\frac{\delta\lambda}{\lambda_0}\right)_{\min} = \frac{1}{\eta_{om}Q_mQ_l}, \quad (1)$$

where  $Q_m$  is the effective mechanical Q factor of OMO,  $Q_l$  is the loaded optical Q, and  $\eta_{om}$  represents the optomechanical transduction factor for sensing whose magnitude depends on laser-cavity detuning, with a value in the order of  $\eta_{om} \sim 1$ . Equation (1) shows clearly that the sensing resolution scales not only with the optical Q of the cavity as what does in conventional microcavity sensors, but also with the effective mechanical Q of OMO. Consequently, in principle, the proposed cavity optomechanical transduction sensing is able to enhance the sensing resolution by about a factor of  $Q_m$  compared with conventional approaches. As we will show below, the mechanical Q of coherent OMO in our device can reach a value above  $10^6$ , resulting in a sensing resolution enhanced by orders of magnitude that is well sufficient for single molecule detection.

As the optomechanical effect is intrinsic to a high-Q microcavity, the proposed approach does not rely on any specific external sensing element attached to the device (*e.g.*, a plasmonic nanoantenna<sup>12–14</sup>), thus capable of fully utilizing the entire effective sensing area offered by a whispering-gallery microcavity which is more than five orders of magnitude larger than that of plasmonic devices. For the same reason, it does not rely on any gain medium, thus universal to different material platforms as long as the device has reasonably high optical Q. On the other hand, this approach is distinctive from the conventional micro-/nano-mechanical sensing<sup>20,21</sup> where the particle detection is realized by monitoring the mechanical frequency shift directly induced by the mass change from particle attaching, which, however, exhibits a minimal detectable mass of  $(\delta m)_{\min} = \frac{2m_{\text{eff}}}{Q_m}$  that relies critically on the motional mass  $m_{\text{eff}}$  and the mechanical Q of the sensor. Although this mechanism was recently applied in combination with optical actuation and readout, it can only detect 2- $\mu\text{m}$ -diameter silica beads with a picogram resolution<sup>22–24</sup>.

## II. RESULTS AND DISCUSSIONS

To verify the above sensing principle, we carried out experiments in a silica microsphere with a diameter of about 100  $\mu\text{m}$ . The device exhibits an intrinsic optical Q as high as  $4.8 \times 10^6$  at a wavelength around 974 nm in the aqueous

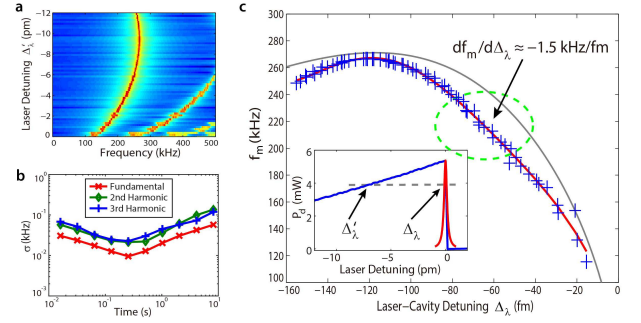


FIG. 2: (a) Spectrogram of cavity transmitted signal as a function of laser wavelength detuning  $\Delta'_\lambda$  (see Fig. 1d for the meaning of  $\Delta'_\lambda$ ), showing the detuning dependent mechanical frequency. The proportional frequency variations at the second and third harmonics are clearly visible. Every spectrum was averaged over 5 traces acquired continuously. (b) The two-sample Allan deviations of the fundamental, second and third harmonic tones measured in DPBS in the absence of sensing particle, showing a minimum deviation of 9.5 Hz at the fundamental oscillation tone. (c) The OMO frequency as a function of laser-cavity wavelength detuning. The blue crosses show the experimental data and the grey curve shows the theory. The red curve is a polynomial fitting to the experimental data. The dashed circle indicates the operating regime for the particle and molecule sensing, with a frequency tuning slope of  $df_m/d\Delta_\lambda = -1.5 \text{ kHz/fm}$  at a laser-cavity detuning of  $\Delta_\lambda = -70 \text{ fm}$ . Inset: Recorded dropped optical power as a function of laser wavelength detuning. This curve was used to obtain the real laser-cavity wavelength detuning  $\Delta_\lambda = \lambda_l - \lambda_0$  where  $\lambda_l$  is the laser wavelength.

environment (Fig. 1c), which is close to the theoretical limit. With such a high optical Q, the optical wave inside the microsphere produces a strong radiation pressure that efficiently actuates the radial breathing mechanical motion of the microsphere (Fig. 1a). Consequently, by dropping an optical power of 3.0 mW into the cavity (Fig. 1d), we are able to boost the mechanical mode above the threshold even in the aqueous environment, resulting in coherent OMO at a frequency of 262 kHz with a mechanical linewidth as narrow as 0.1 Hz (Fig. 1f), corresponding to an effective mechanical Q of  $2.6 \times 10^6$ . As shown in Fig. 1e, the significant optomechanical oscillation leads to a harmonic comb on the power spectrum of the cavity transmission, a feature of coherent OMO resulting from the nonlinear transduction of the optical cavity<sup>25,26</sup>.

In particular, the strong optical spring effect from the optomechanical coupling results in an OMO frequency sensitively dependent on the laser-cavity detuning (Fig. 2a). As shown in Fig. 2c, when the laser-cavity wavelength detuning decreases from  $-150 \text{ fm}$ , the OMO frequency increases from 247 kHz to a peak value of 267 kHz, and then decreases quickly to about 115 kHz when the laser wavelength is tuned close to the center of cavity resonance, with a tuning slope of  $df_m/d\Delta_\lambda \approx -1.5 \text{ kHz/fm}$  at a laser-cavity detuning of  $\Delta_\lambda \approx -70 \text{ fm}$ . The observed optical spring follows closely the theoretical expectation (grey curve in Fig. 2c).

Such an optical spring corresponds to a sensitive *optical-to-mechanical frequency transduction*, inferring that every 1-fm

cavity resonance wavelength shift induced by a particle binding event can be transduced to an OMO frequency change of about 1.5 kHz that is about four orders of magnitude larger than the linewidth of optomechanical oscillation (Fig. 1f). A detailed characterization of the Allan deviation of the OMO frequency (Fig. 2b) shows a minimum two sample deviation of 9.5 Hz at the fundamental OMO frequency, implying a detection resolution of  $\delta\lambda/\lambda_0 \approx 6 \times 10^{-12}$  in the device. This record resolution clearly shows the powerfulness of the demonstrated approach, which is more than  $10^4$  times higher than a conventional microcavity sensor with the same optical  $Q^{10}$ . It is even about 50 times higher than that achieved with an optical  $Q$  of  $10^8$  at a visible wavelength<sup>5</sup>. Note that the harmonics of the optomechanical oscillation vary proportionally with the OMO fundamental frequency (Fig. 2a) and thus can also be applied for particle sensing. Although this does not improve the sensing resolution due to the same SNR of detection, in practice, the larger frequency shifts on the higher-order harmonics significantly facilitate the mechanical spectrum analysis (by allowing to use a coarser resolution bandwidth), which reduces considerably the excessive detection noises from consecutive multiple particles skimming by the cavity surface.

To characterize the real sensing performance, we performed the sensing experiments on silica nanobeads with different diameters. We set the laser-cavity detuning at the operational point indicated within the dashed circle of Fig. 2c and delivered silica nanobeads diluted in Dulbecco's Phosphate-Buffered Saline (DPBS) around the microsphere. The particle binding events were recorded by searching the sudden changes of the oscillation frequency in the recorded spectrograms. Typical examples are shown in Fig. 3a-d for the nanobeads with radii of 11.6, 25, 50, and 85-nm, respectively. Here in the case of 11.6-nm beads, the frequency steps were recorded at the third harmonic of the oscillation frequency while all others were obtained at the fundamental. As shown in Fig. 3a, a clear step of  $1.3 \pm 0.1$  kHz (corresponding to  $0.43 \pm 0.03$  kHz step at the fundamental oscillation tone) was observed at the time of 58 second with an SNR of 13. An increase of the oscillation frequency implies a red shift of the cavity resonance wavelength, which corresponds to a binding of a 11.6-nm silica bead on the surface of the microsphere. Figures 3b-d show frequency steps of  $-1.7 \pm 0.3$ ,  $3.5 \pm 0.9$ , and  $6.8 \pm 0.4$  kHz, respectively, which correspond to the binding (positive frequency steps) or unbinding (negative steps) events of 25-nm, 50-nm, and 85-nm beads.

To obtain the statistical properties of the binding events, we recorded a total number of 500121, 521389, 1335415, and 758728 spectra in sensing 11.6-nm, 25-nm, 50-nm, and 85-nm beads, respectively, among which frequency steps of 1690, 2043, 2685, and 2558 were captured with the SNR exceeding unity. Figures 3e-h show the histograms of the normalized frequency steps,  $\delta f_m/f_m$ , which indicate maximum OMO frequency shifts of  $\delta f_m/f_m = (1.4 \pm 0.4) \times 10^{-3}$ ,  $(-7.8 \pm 1.5) \times 10^{-3}$ ,  $(1.3 \pm 0.3) \times 10^{-2}$ , and  $(-2.3 \pm 0.6) \times 10^{-2}$ , respectively, for beads with radii of 11.6, 25, 50, and 85 nm. We converted the recorded OMO frequency steps into the corresponding cavity resonance wave-

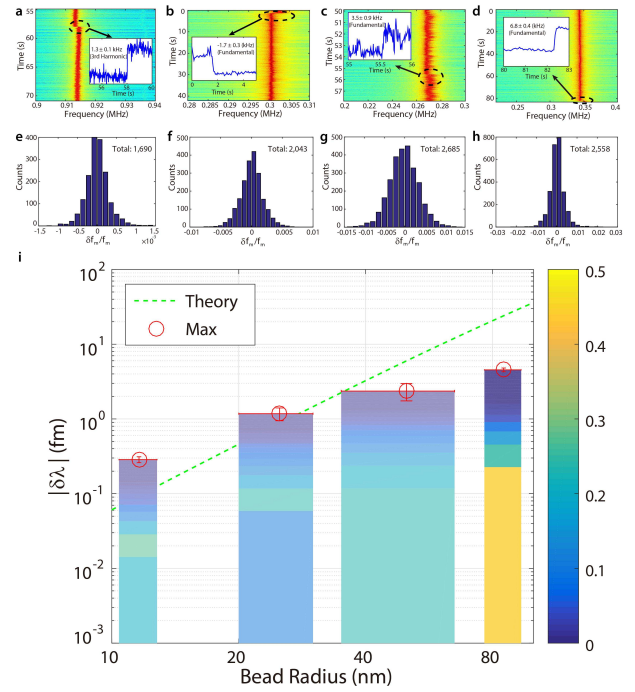


FIG. 3: (a)-(d) Typical mechanical spectrograms for the binding events of silica beads with average radii of 11.6, 25, 50, and 85 nm, where (a) shows that of third harmonic and (b)-(d) show those of the fundamental oscillation frequency. The insets show the detailed frequency steps. (e)-(h) The histograms of the normalized frequency steps  $\delta f_m/f_m$ . (i) The corresponding cavity resonance shifts induced by the particle binding as a function of bead radius. The color bars show the probability density functions of the recorded cavity resonance wavelength shifts induced by particle binding, where the bar width indicates the standard deviation of the bead size (provided by the manufacturer) and the color map indicates the magnitude of probability density. The red circles indicate the recorded maximum wavelength shifts of the cavity resonance. The dashed curve shows the theoretical prediction<sup>27</sup>.

length shifts  $\delta\lambda$ , with the transduction rate of  $df_m/d\Delta\lambda = -1.5$  kHz/fm. The probability density function of their absolute values are plotted as color bars in Fig. 3i, with maximum wavelength shifts of  $|\delta\lambda|/\lambda_0 = 2.6 \times 10^{-10}$ ,  $1.2 \times 10^{-9}$ ,  $2.4 \times 10^{-9}$ , and  $4.6 \times 10^{-9}$ , respectively, for the four bead sizes (red circles). For comparison, we also numerically estimated the expected maximum wavelength change as a function of bead radius (green dashed line)<sup>27</sup>. The experiment results agree with the theoretical predictions when the bead size is small (11.6-nm and 25-nm). At larger bead radii (50-nm and 85-nm), the experiment values are smaller than the theoretical predictions, which is because the optical  $Q$  starts to degrade at a large beam size. As the optical spring depends on both the laser-cavity detuning and the optical  $Q$ , the impact from cavity  $Q$  change counteracts that from the cavity resonance wavelength shift, leading to a smaller shift of OMO frequency

The ultrahigh detection sensitivity demonstrated on silica nanobeads readily implies the superior capability of sensing single protein molecules. To do so, we injected BSA diluted

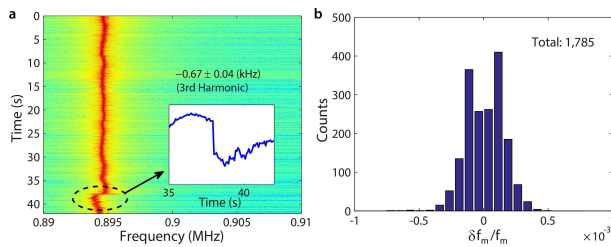


FIG. 4: (a) A typical mechanical spectrogram recorded at the third harmonic of the oscillation tone, capturing the event of a BSA protein molecule detaching from the silica microsphere surface at 38 second, with a clear frequency step (inset) of  $-0.67 \pm 0.04$  kHz. (b) The histogram of the normalized frequency steps.

in DPBS around the microsphere sensor, with the concentration gradually increased from 1 nM to 10 nM. In the protein sensing experiment, the excessive noises from the unwanted molecules were significantly reduced, resulting in a detection noise level close to the DPBS background noise obtained from the Allan deviation measurement. The third order harmonic of the oscillation frequency was employed to monitor the frequency steps. As shown in Fig. 4a, a maximum frequency step of  $-0.67 \pm 0.04$  kHz was observed with an SNR of 16.8, which corresponds to a  $-0.22 \pm 0.01$  kHz at the fundamental oscillation tone. In total, we recorded 145407 spectra among which 1785 frequency steps were captured. The histogram of the normalized frequency steps is plotted in Fig. 4b, with the maximum step of  $\delta f_m / f_m = (-7.6 \pm 0.4) \times 10^{-4}$  which corresponds to a cavity resonance shift of  $|\delta \lambda| / \lambda_0 = 1.5 \times 10^{-10}$ . This observation clearly proves the capability of sensing single BSA molecule with a molecule weight of 66 kDalton. By assuming the resonance shift is proportional to the mass (or equivalently, to the volume) of the protein<sup>27</sup>, we derive that our current setup is capable of detecting proteins as small as

3.9 kDalton with an SNR above unity.

### III. CONCLUSION

The demonstrated single molecule detection now paves the foundation of ultra-sensitive cavity optomechanical transduction sensing. The sensing resolution can be further improved significantly in the future. For example, the minimal detectable OMO frequency shift in current devices is primarily limited by the laser frequency jitter in our experiment. With an OMO linewidth of only  $\sim 0.1$  Hz, we expect that the future adoption of a fine laser frequency locking circuitry can further improve the sensing resolution by  $\sim 100$  times to around  $\delta \lambda / \lambda_0 \sim 10^{-14}$ . On the other hand, the optical Q can be increased to above  $10^8$  if a visible laser is employed<sup>5</sup>, which would further improve the sensing resolution by more than one order of magnitude. Moreover, a plasmonic structure can also be incorporated to enhance the cavity resonance shift. These future improvements would enable detecting small molecules and atoms with a mass down to sub-Dalton level, with a great potential for dramatically advancing the capability of biosensing to an unprecedented level.

In particular, as the molecule binding occurs during the coherent mechanical motion of the sensor, controlling the motion pattern of the coherent OMO (amplitude, phase, time waveform, etc.) may function as a unique paradigm to study/control the mechanical properties of molecule binding/unbinding. This, in combination with certain functionalization of the sensor surface<sup>2</sup> and with implementation of potentially versatile optomechanical motions<sup>19</sup>, may offer a unique multifunctional biomolecule toolbox that is not only able to observe cellular machineries at work, but also to selectively manipulate single-molecule interactions<sup>28</sup>.

- <sup>1</sup> Serpengüzel, A., Griffl, G. & Arnold, S. Excitation of resonances of microspheres on an optical fiber. *Opt. Lett.* **20**, 654–656 (1995).
- <sup>2</sup> Vollmer, F. & Arnold, S. Whispering-gallery-mode biosensing: label-free detection down to single molecules. *Nature Methods* **5**, 591–596 (2008).
- <sup>3</sup> Fan, X. *et al.* Sensitive optical biosensors for unlabeled targets: A review. *Analytica Chimica Acta* **620**, 8–26 (2008).
- <sup>4</sup> Boyd, R. W. & Heebner, J. E. Sensitive disk resonator photonic biosensor. *Appl. Opt.* **40**, 5742–5747 (2001).
- <sup>5</sup> Lu, T. *et al.* High sensitivity nanoparticle detection using optical microcavities. *Proceedings of the National Academy of Sciences* **108**, 5976–5979 (2011).
- <sup>6</sup> Knittel, J., Swaim, J. D., McAuslan, D. L., Brawley, G. A. & Bowen, W. P. Back-scatter based whispering gallery mode sensing. *Scientific Reports* **3**, 2974 (2013).
- <sup>7</sup> Avino, S. *et al.* Direct sensing in liquids using whispering-gallery-mode droplet resonators. *Advanced Optical Materials* **2**, 1155–1159 (2014).
- <sup>8</sup> Lu, T., Su, T.-T. J., Vahala, K. J. & Fraser, S. Split frequency sensing methods and systems. *US Patent* US 8,593,638 B2 (2013).
- Preliminary filing in Oct. 2008.
- <sup>9</sup> Zhu, J. *et al.* On-chip single nanoparticle detection and sizing by mode splitting in an ultrahigh-Q microresonator. *Nature Photonics* **4**, 46–49 (2010).
- <sup>10</sup> White, I. M. & Fan, X. On the performance quantification of resonant refractive index sensors. *Opt. Express* **16**, 1020–1028 (2008).
- <sup>11</sup> Min, B. *et al.* High-Q surface plasmon polariton whispering gallery microcavity. *Nature* **457**, 455–458 (2009).
- <sup>12</sup> Shopova, S. I., Rajmangal, R., Holler, S. & Arnold, S. Plasmonic enhancement of a whispering-gallery-mode biosensor for single nanoparticle detection. *Appl. Phys. Lett.* **98**, 243104 (2011).
- <sup>13</sup> Dantham, V. R. *et al.* Label-free detection of single protein using a nanoplasmonic-photonic hybrid microcavity. *Nano Letters* **13**, 3347–3351 (2013).
- <sup>14</sup> Baaske, M. D., Foreman, M. R. & Vollmer, F. Single-molecule nucleic acid interactions monitored on a label-free microcavity biosensor platform. *Nature Nanotechnology* (2014).
- <sup>15</sup> Kippenberg, T. J. & Vahala, K. J. Cavity optomechanics: Back-action at the mesoscale. *Science* **321**, 1172–1176 (2008).
- <sup>16</sup> Marquardt, F. & Girvin, S. M. Optomechanics. *Physics* **2**, 40

- (2009).
- 17 Favero, I. & Karrai, K. Optomechanics of deformable optical cavities. *Nature Photon.* **3**, 201–205 (2009).
  - 18 Thourhout, D. V. & Roels, J. Optomechanical device actuation through the optical gradient force. *Nature Photonics* **4**, 211–217 (2010).
  - 19 Aspelmeyer, M., Kippenberg, T. J. & Marquardt, F. Cavity optomechanics. *Rev. Mod. Phys.* **86**, 1391–1452 (2014).
  - 20 Waggoner, P. S. & Craighead, H. G. Micro- and nanomechanical sensors for environmental, chemical, and biological detection. *Lab on a Chip* **7**, 1238 (2007).
  - 21 Arlett, J. L., Myers, E. B. & Roukes, M. L. Comparative advantages of mechanical biosensors. *Nature Nanotech.* **6**, 203 (2011).
  - 22 Liu, F. & Hossein-Zadeh, M. Mass sensing with optomechanical oscillation. *Sensors Journal, IEEE* **13**, 146–147 (2013).
  - 23 Kim, K. H. & Fan, X. Surface sensitive microfluidic optomechanical ring resonator sensors. *Appl. Phys. Lett.* **105**, 191101 (2014).
  - 24 Forstner, S. *et al.* Cavity optomechanical magnetometer. *Phys. Rev. Lett.* **108**, 120801 (2012).
  - 25 Hossein-Zadeh, M., Rokhsari, H., Hajimiri, A. & Vahala, K. J. Characterization of a radiation-pressure-driven micromechanical oscillator. *Physical Review A* **74**, 023813 (2006).
  - 26 Xiong, C., Sun, X., Fong, K. Y. & Tang, H. X. Integrated high frequency aluminum nitride optomechanical resonators. *Appl. Phys.* **100**, 171111 (2012).
  - 27 Arnold, S., Khoshshima, M., Teraoka, I., Holler, S. & Vollmer, F. Shift of whispering-gallery modes in microspheres by protein absorption. *Opt. Lett.* **28**, 272–274 (2003).
  - 28 Müller, D. J. & Dufrene, Y. F. Atomic force microscopy as a multifunctional molecular toolbox in nanobiotechnology. *Nature Nanotech.* **3**, 261 (2008).

**Acknowledgements** The related contents are pending for patent application. W.Y. and T.L. acknowledge the support from NSERC Discovery and CFI LOF funds. W.C.J. and Q.L. acknowledge the support from the DARPA QuASAR program.

**Author Contributions** W.Y. fabricated the devices, prepared the samples, and performed the experiments. W.C.J. and Q.L. discovered the sensing principle and mechanism, developed the theory, and conducted the numerical simulation. T. L. conceived and designed the experiments, developed software to control the experiments, and processed the data. Q.L. and T.L. conceived the concept and supervised the project. W.Y., W.C.J., Q.L., and T.L. worked together on the result analysis/interpretation and manuscript preparation.

**Author Information** The authors declare no competing financial interests. Correspondence and requests for materials should be addressed to T.L. ([taolu@ece.uvic.ca](mailto:taolu@ece.uvic.ca)) and Q.L. ([qiang.lin@rochester.edu](mailto:qiang.lin@rochester.edu)).